Quad-Band U-Slot Antenna for Mobile Applications

Eduardo de las HERAS PALMERO, Zbyněk RAIDA, Roberto LAMADRID RUIZ

Dept. of Radio Electronics, Brno University of Technology, Purkyňova 118, 612 00 Brno, Czech Republic

eherasp@hotmail.com, raida@feec.vutbr.cz, roberto_lamadrid@hotmail.com

Abstract. *In this paper, two different planar quad-band antennas are designed, modeled, fabricated and measured. Subsequently, the antennas are redesigned using an electromagnetic band gap substrate (EBG). Those new planar antennas operate in four frequency bands: 900 MHz, 1 800 MHz (both GSM), 1 900 MHz (USA) and 2 400 to 2 500 MHz (Bluetooth) The antenna has four narrow U-shaped slots etched to the patch. Using software, CST Microwave Studio [1], Zeland IE3D [2], and FEMLAB [3], simulations have been carried out to investigate the antenna's performance and characteristics. The antennas designed have been also built and measured to compare the real results with those obtained from the simulations.*

Keywords

Multi-band planar antennas, perturbation slots, modal analysis, full-wave analysis, GSM, Bluetooth. EBG substrates.

1. Introduction

Microstrip patch antennas are commonly used in mobile communications terminals due to their many attractive features, such as a simple structure, low production costs, light weight, and robustness [4], [5].

Patch antennas consist of a rectangular antenna element in a small distance from a planar reflector. In order to reduce dimensions of the antenna and simplify the fabrication process, patch antennas are usually done from teflon-based microwave substrates exhibiting very low electrical losses [4], [5]. A basic patch antenna can be tuned to achieve more operation bands. This can be done by adding perturbation slots. There are other possibilities to get multi-band antennas like using fractal approaches, planar radiators in different distances from the ground plane, etc. But this paper is focused in the first approach only.

Once the antennas have been design, a narrow bandwidth is evidently their major disadvantage (in some cases, this value is lower than 1 %). With the intention to overcome this handicap, a thick, high permittivity substrate is used, and potential surface waves are suppressed applying so called Electromagnetic Band Gap (EBG).

The surface wave propagation is a serious problem of microstrip antennas. Surface waves reduce antenna efficiency and gain, limit bandwidth, increase end-fire radiation and cross-polarization levels, and narrow the applicable frequency range of microstrip antennas. Additionally, the miniaturization of microstrip antennas and their integration with microstrip circuits is hindered because high dielectric substrates are required to achieve these objectives. To avoid this, the substrate is periodically loaded so that the surface waves cannot propagate along the substrate. Also, other surface wave coupling effects like mutual coupling between array elements and interference with board systems can be suppressed [6]–[15].

In the open literature, no information about EBG antennas in the frequency range from 0.8 GHz to 2.5 GHz has been published yet. Hence, the numerical values of the parameters of EBG substrates were proposed empirically.

Once the proper EBG substrate was selected for the surface wave suppression, the design of an EBG antenna has been straightforward: the metallic antenna layout has been surrounded by an EBG lattice, and the layout dimensions has been recomputed in a conventional way (the EBG substrate does not interfere with the near field of the antenna, and it suppresses the surface waves, which are not included in the patch antenna design [6]–[15]).

2. Antenna Design

In this section, the dimension of the antennas and their structural characteristics are considered. All the antennas have been built using Arlon 25N substrate (dielectric constant is $\varepsilon_r = 3.28$, substrate height $h = 3.08$ mm).

Dimensions of the first prototype on a conventional substrate are given in Fig. 1a, meanwhile the second prototype is shown in Fig 1b. The metallic parts are painted in gray; the dielectric substrate without the metallization is shown in white. Both antennas are fed by a coaxial probe. In the first case, the feeding point is situated in $x = -4$ mm, $y = 28.5$ mm being the reference point the center of the antenna. For the second antenna, the feeding point is situated in $x = -4$mm, $y = 23.5$ mm. In all the cases, the widths of the slots are 1 mm.

In Fig. 2a, we can see the first prototype redesign with an EBG substrate using the honeycomb configuration. In Fig. 2b, the second prototype is shown using the square lattice configuration. The numerical values of the parameters of EBG substrates were proposed empirically: the holes dis-

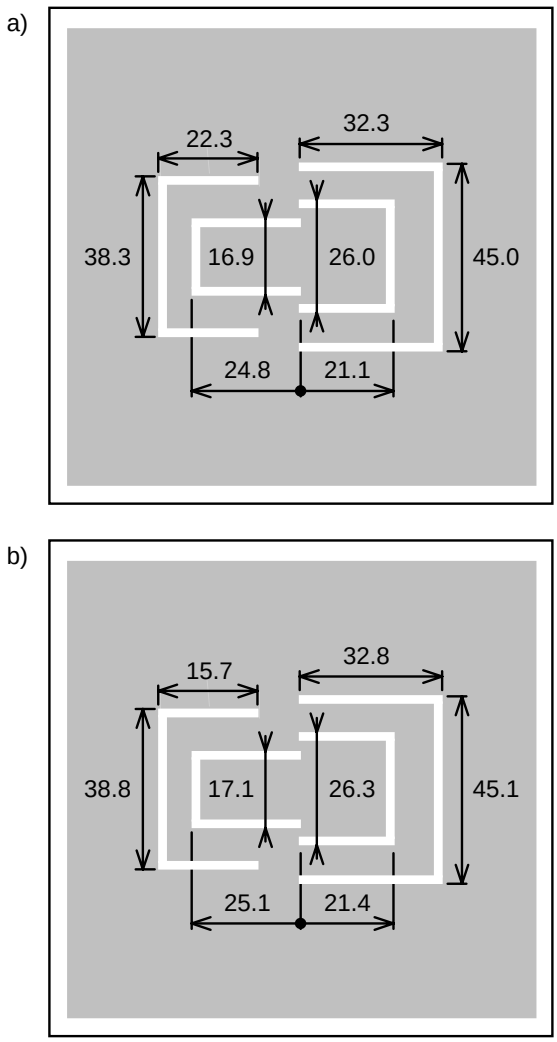

Fig. 1. Dimensions (in millimeters) of the layout of the investigated antennas. a) The prototype 1 – the patch width is 108.0 mm, and the patch height 112.5 mm. b) The prototype 2 – the patch width is 109.4 mm, and the patch height 114.0 mm. Dimensions are measured from the centers of slots.

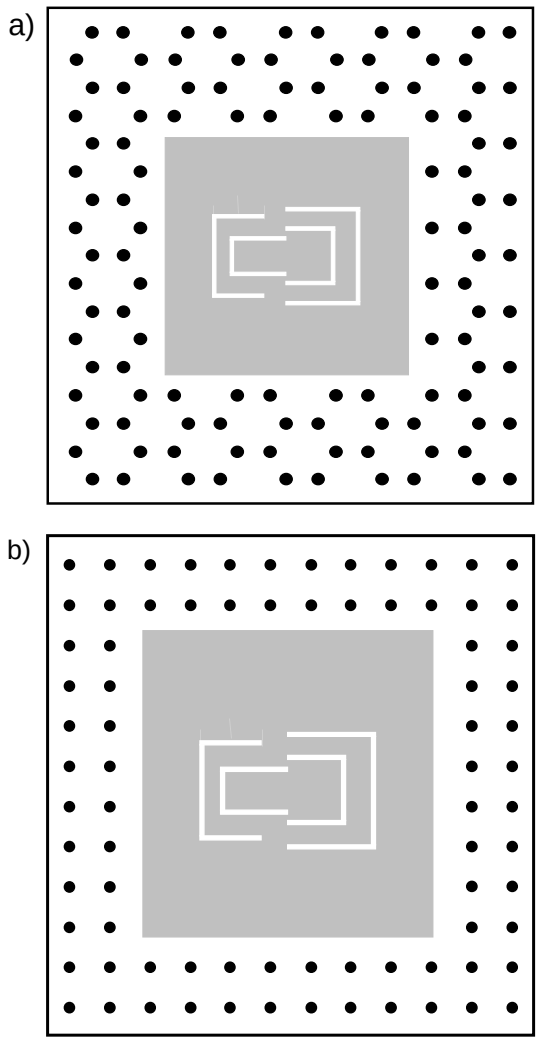

Fig. 2. Layout of the antennas on the EBG substrates. a) The prototype 1 – the honeycomb lattice: the distance between the sides of hexagons is a = 15 mm, the radius of holes is 5 mm. b) The prototype 2 – the square lattice: the distance between the sides of squares is a = 15 mm, the radius of holes is 5 mm. Dimensions of patches and slots are identical with those ones given in Fig. 1.

tance was set to a = 15 mm, and the radius of the holes was set to r = 2 mm.

The holes were drilled into the substrate in two different configurations. First, the ground plane stayed continuous, and second, the ground plane was perforated together with dielectrics. Both the simulation and the experiment did not reveal any difference in the behavior of those two configurations.

3. Cavity Model

In order to investigate resonances of the antennas of interest, the cavity model is built. The antennas are modeled like a longitudinally homogeneous dielectric waveguide which cross section is identical with the shape of the antenna element. Permittivity of the waveguide equals to the permittivity of the antenna substrate. Side walls of the waveguide are assumed to be perfectly magnetic conductive.

In the waveguide, the propagation of the transversally magnetic modes is assumed. The analysis is based on computing the distribution of the longitudinal component of the electric field intensity, which is perpendicular both to the ground plane and to the planar antenna element. The analysis is performed in FEMLAB 3.1.

Results of the modal analysis of the prototype 1 are depicted in Fig. 4:

a) The obtained resonant frequency 0.653 GHz deviates for 27 % from the required one (0.9 GHz). The maximum of the current appears between the U-slots. Considering the whole patch, the dominant mode TM_{10} can be identified shifted to the left part of the patch.

b) The obtained frequency 1.816 GHz deviates for 1 % from the required one (1.8 GHz). The dominant mode TM_{10} appears inside the internal region of slots.

c) The obtained frequency 1.957 GHz exhibits 2.6 % deviation from the required frequency (1.9 GHz). The current distribution is mainly concentrated in between the exterior U-slots and the interior ones: the distribution is close to the mode TM_{11}.

d) The obtained frequency 2.439 GHz deviates for 1.6 % compared to the required one (2.5 GHz). The current corresponds to a higher-order mode.

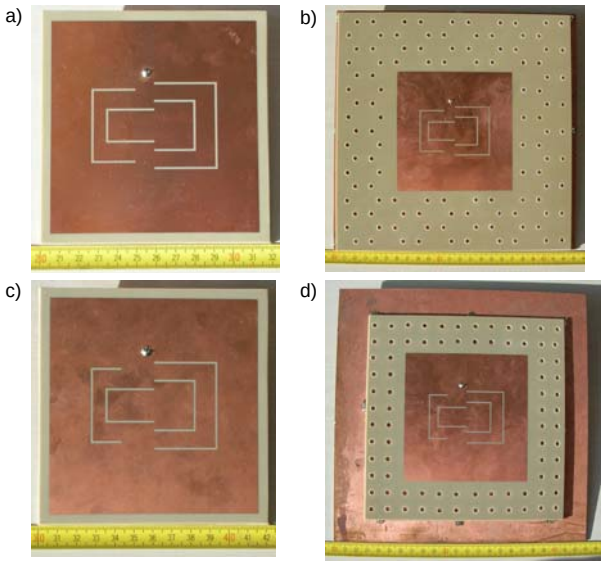

Fig. 3. Photographs of the fabricated prototypes of designed antennas: Prototype 1 on the conventional substrate (a) and the EBG one (b). Prototype 2 on the conventional substrate (c) and the EBG one (d).

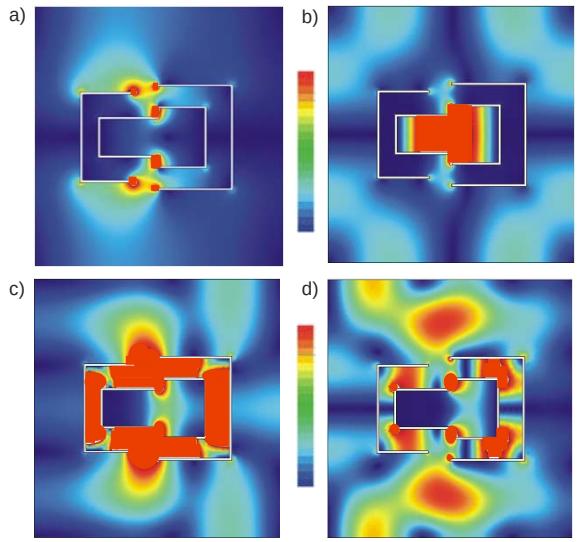

Fig. 4. Current distribution of the prototype 1 on the conventional substrate. The operating frequency: a) 0.653 GHz, b) 1.816 GHz, c) 1.957 GHz, d) 2.439 GHz.

Results of the modal analysis of the prototype 2 are depicted in Fig. 5:

a) The obtained resonant frequency is 0.684 GHz, which deviates for 24 % from the required operation frequency (0.9 GHz). The current is very similar to the basic mode TM_{10} of the prototype 1.

b) The obtained frequency is 1.527 GHz, i.e. the deviation is 15 % (1.8 GHz). In this case, the current is concentrated in the interior of the smaller U-slots (similar to the mode TM_{12} of the whole patch).

c) The obtained frequency (1.721 GHz) deviates for 9.4 % (1.9 GHz). For this band, the current is mainly concentrated in between the U-slots (a higher mode).

d) The obtained frequency is 2.43 GHz; thus the deviation is 0.81 % compared to the required frequency (2.45 GHz). The current distribution corresponds to a higher-order mode.

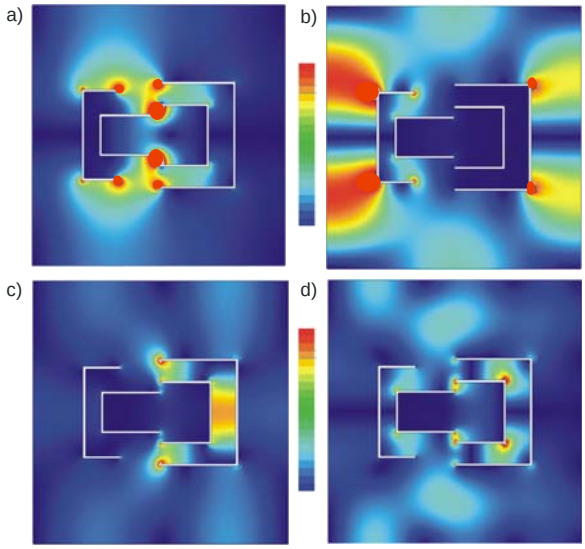

Fig. 5. Current distribution of the prototype 2 on the conventional substrate. The operating frequency: a) 0.684 GHz, b) 1.527 GHz, c) 1.721 GHz, d) 2.430 GHz.

In the following section, results of the modal analysis are verified by the full-wave analysis and measurements.

4. Full-Wave Analysis, Measurement

For the full-wave analysis of antennas on conventional substrates, Zeland IE3D is used. Due to the moment method computational kernel of IE3D, analyses are performed efficiently and accurately.

On the other hand, gaps in EBG substrates require a novel formulation of Green's functions describing the relation between currents and charges on one hand, and potentials (vector, scalar) on the other hand. Therefore, Zeland IE3D can hardly be used for that type of the analysis (version 10 allows to treat finite dielectric volumes, but the analysis is CPU-time demanding). Antennas on EBG substrates are therefore analyzed by CST Microwave Studio.

In the following paragraphs, we discuss current distributions computed by the full-wave analysis, and compare them with the results of cavity models. Frequency res-

ponses of the reflection coefficient are computed by Zeland IE3D (conventional substrates) and CST Microwave Studio (EBG substrates), and are compared to measurements results. Finally, measured directivity patterns of all the antennas in all the operation bands are presented here.

4.1 Prototype 1, Conventional Substrate

In Fig. 6, vector current distributions on the antenna element of the prototype 1 on the conventional substrate are depicted. Comparing current magnitudes with the results of the modal analysis, a quite good correspondence can be observed. Differences are mostly given by feeding the antenna.

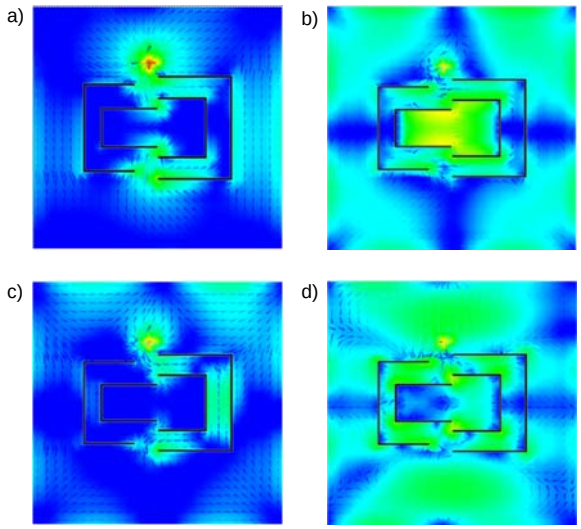

Fig. 6. Current distribution of the prototype 1 on the conventional substrate. The operating frequency: a) 0.85 GHz, b) 1.80 GHz, c) 1.94 GHz, d) 2.45 GHz. Computed by Zeland IE3D.

Comparing resonant frequencies of the modal analysis and the full-wave one, following relative errors are obtained: 5.5 % – the first band, 0.0 % – the second band, 2.1 % – the third band, 0.0 % – the fourth band.

Dealing with current vectors, the situation is much more complicated here. In the first operation band and the second one, strong vertical current components are excited, which results in very poor values of the cross-polarization (see Tab. 1). In higher operation bands, current distributions are rather complex, and therefore, a direct relation between currents and polarization properties can be hardly found. Nevertheless, the resultant polarization properties are better in higher bands (see Tab. 1).

Frequency	Cross-polarization
0.90 GHz	– 0.5 dB
1.80 GHz	– 8.5 dB
1.90 GHz	– 12.6 dB
2.45 GHz	– 11.0 dB

Tab. 1. Cross-polarization values for the prototype 1 on the conventional substrate. Computed by Zeland IE3D.

In Fig. 7, frequency response of the reflection coefficient computed by CST Microwave Studio and the measured one are depicted. Comparing computed resonant frequencies (full-wave) and measured ones, following relative errors are obtained: 3.5 % – the first band, 0.0 % – the second band, 2.3 % – the third band, 4.1 % – the fourth band.

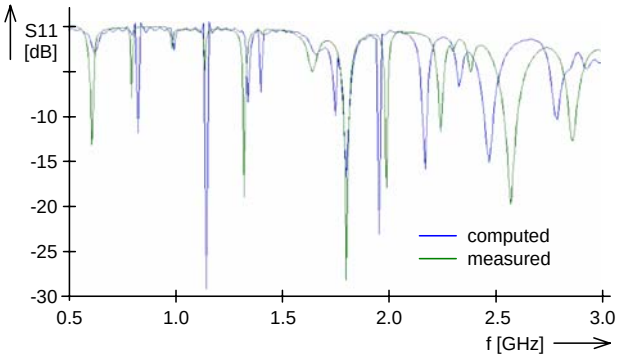

Fig. 7. Frequency course of the reflection coefficient for the prototype 1 on the conventional substrate (blue – computed by CST Microwave Studio, green – measured).

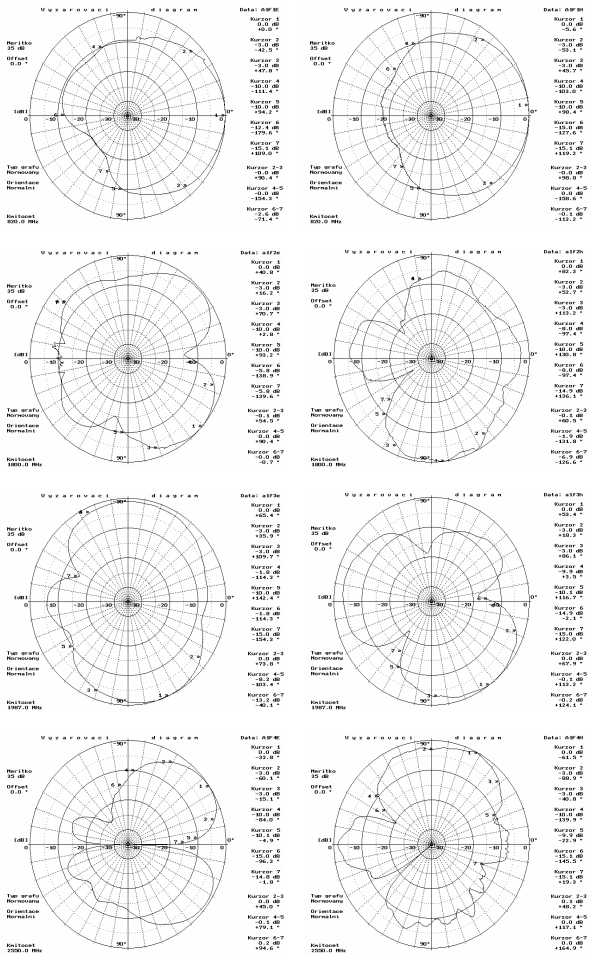

Fig. 8. Measured directivity patterns of the prototype 1 on the conventional substrate in the E-plane (left), and the H-plane (right), for each frequency band (0.820 GHz, 1.800 GHz, 1.987 GHz, 2.550 GHz), respectively.

Rather complicated current distributions result in problematic directivity patterns: there is the minimum of radiation in the normal direction in the second operation band and the fourth one in the E-plane, and in the third operation band in the H-plane.

Due to all the mentioned reasons, the antenna was redesigned by tuning the layout dimensions.

4.2 Prototype 2, Conventional Substrate

In Fig. 6, vector current distributions on the antenna element of the prototype 2 on the conventional substrate are depicted. Current magnitudes correspond well with the modal analysis. Comparing resonant frequencies of the modal analysis and the full-wave one, following relative errors are obtained: 4.4 % – the first band, 0.5 % – the second band, 0.5 % – the third band, 0.0 % – the fourth band.

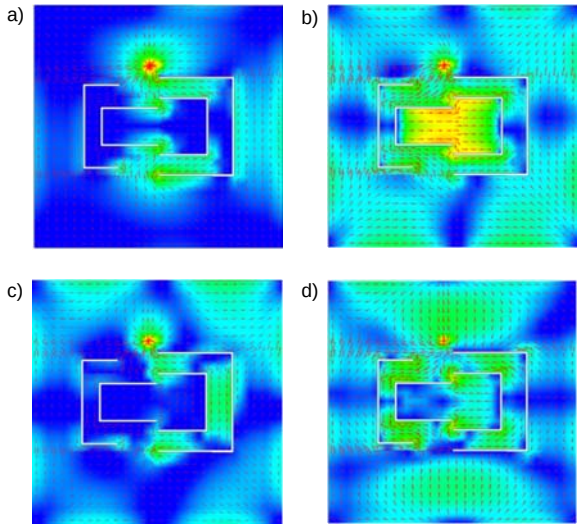

Fig. 9. Current distribution of the prototype 2 on the conventional substrate. The operating frequency: a) 0.86 GHz, b) 1.79 GHz, c) 1.91 GHz, d) 2.45 GHz. Computed by Zeland IE3D.

Observing current vectors, horizontal components are stronger here, and the vertical ones tend to mutually compensate resulting in better cross-polarization values (see Tab. 2).

Frequency	Cross-polarization
0.90 GHz	-11.0 dB
1.80 GHz	-13.7 dB
1.90 GHz	-12.0 dB
2.45 GHz	- 13.4 dB

Tab. 2. Cross-polarization values for the prototype 2 on the conventional substrate. Computed by Zeland IE3D.

In Fig. 10, frequency response of the reflection coefficient computed by CST Microwave Studio and the measured one are depicted. Comparing computed resonant frequencies (full-wave) and measured ones, following relative errors are obtained: 7.0 % – the first band, 0.3 % – the second one, 2.1 % – the third one, 0.4 % – the fourth one.

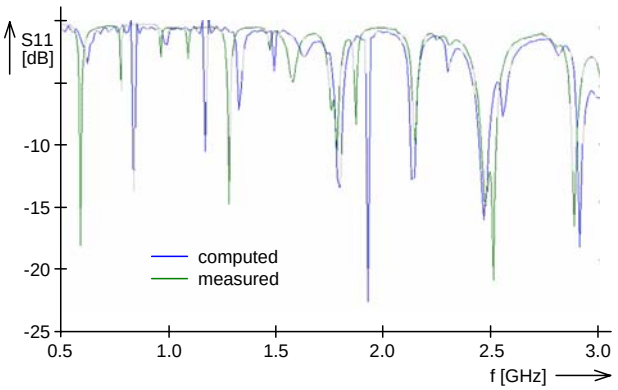

Fig. 10. Frequency course of the reflection coefficient for the prototype 2 on the conventional substrate (blue – computed by CST Microwave Studio, green – measured).

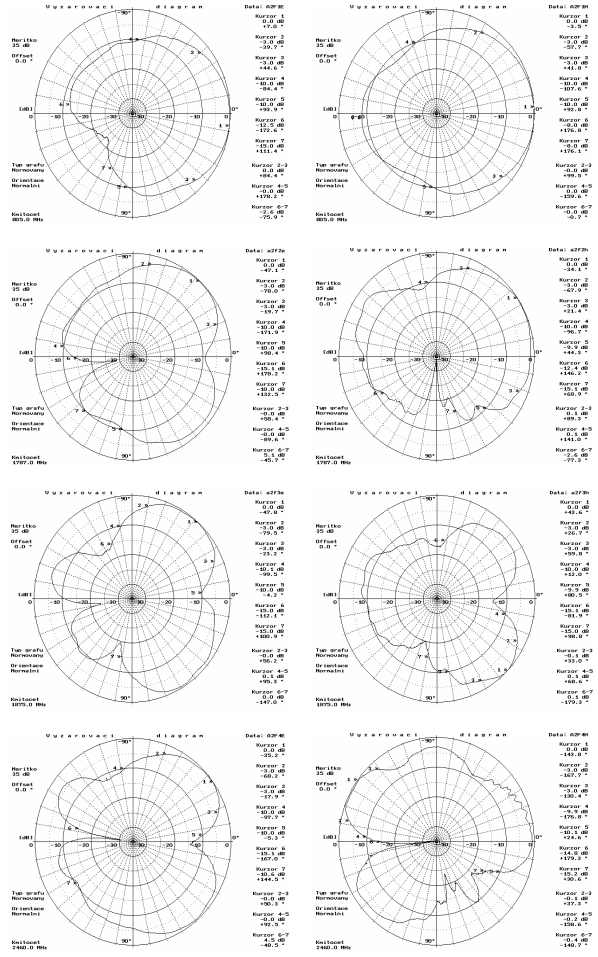

Fig. 11. Measured directivity patterns of the prototype 2 on the conventional substrate in the E-plane (left), and in the H-plane (right), for each frequency band (0.805 GHz, 1.787 GHz, 1.875 GHz, 2.460 GHz), respectively.

The performed tuning improved the directivity patterns also: the radiation minims are kept in the normal direction, but they do not significantly exceed the level of –10 dB (compared to –30 dB in the previous case). The symmetry of patterns is improved, too. A further improvement is going to be reached by using EBG substrates.

4.3 Prototype 1, EBG Substrate

In Fig. 12, magnitude current distributions on the antenna element of the prototype 1 on the honeycomb lattice EBG substrate are depicted. Replacing the conventional substrate by the honeycomb lattice EBG one has not influenced the distribution of currents.

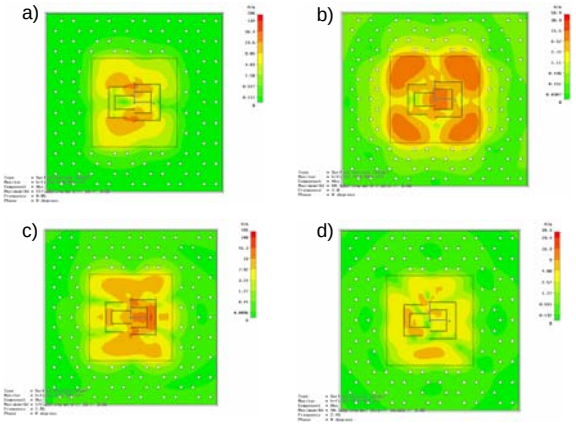

Fig. 12. Current distribution of the prototype 1 on the EBG substrate. The operating frequency: a) 0.86 GHz, b) 1.79 GHz, c) 1.91 GHz, d) 2.45 GHz. Computed by CST Microwave Studio.

Dealing with polarization properties, cross-polarization values in operation frequency bands are given in Tab. 3. Obviously, replacing the conventional substrate by the honeycomb lattice EBG one significantly improved the polarization properties.

Frequency	Cross-polarization
0.90 GHz	-11.6 dB
1.80 GHz	-10.1 dB
1.90 GHz	-11.6 dB
2.45 GHz	-15.4 dB

Tab. 3. Cross-polarization for the prototype 1 on the honeycomb lattice EBG substrate. Computed by CST Microwave Studio.

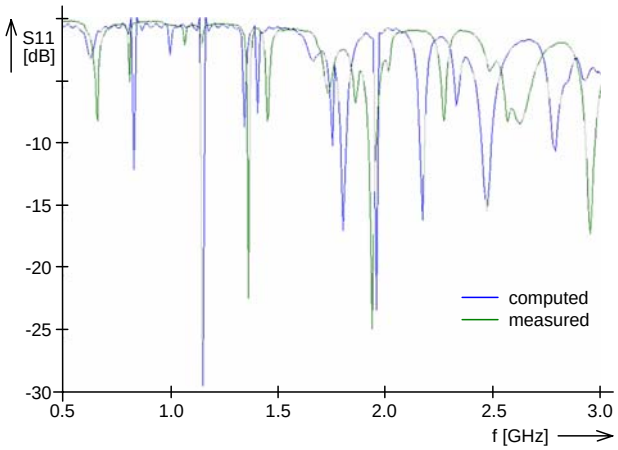

Fig. 13. Frequency response of the reflection coefficient for the prototype 1 on the honeycomb lattice EBG substrate (blue – computed by CST Microwave Studio, green – measured).

Comparisons of the reflection coefficients computed by CST Microwave Studio and measured in an anechoic chamber are given in Fig. 13. Following deviations between results have been obtained: 2.8 % – the first band, 3.7 % – the second one, 0.4 % – the third one, 4.3 % – the fourth one.

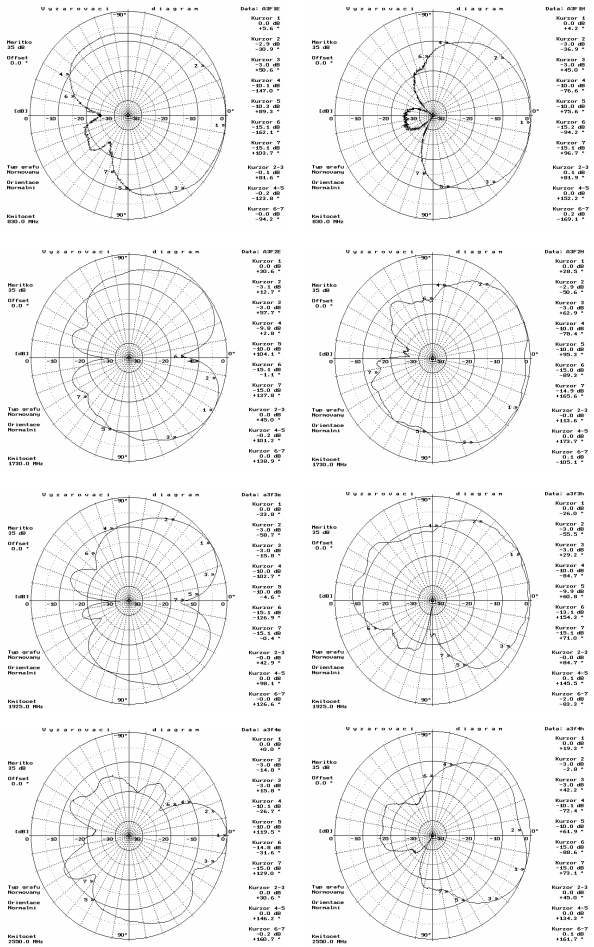

Fig. 14. Measured directivity patterns of the prototype 1 on the EBG substrate in the E-plane (left), and in the H-plane (right), for each frequency band (0.830 GHz, 1.730 GHz, 1.925 GHz, 2.550 GHz), respectively.

Utilization of the EBG substrate positively influenced the directivity patterns, also: symmetry of patterns has been improved, and minims in the normal direction do not significantly exceed the level of –10 dB. For that reason, the EBG approach has been applied to the tuned prototype 2, also.

4.4 Prototype 2, EBG Substrate

In Fig. 15, magnitude current distributions on the antenna element of the prototype 2 on the square lattice EBG substrate are depicted. Replacing the conventional substrate by the square lattice EBG one has not influenced the distribution of currents.

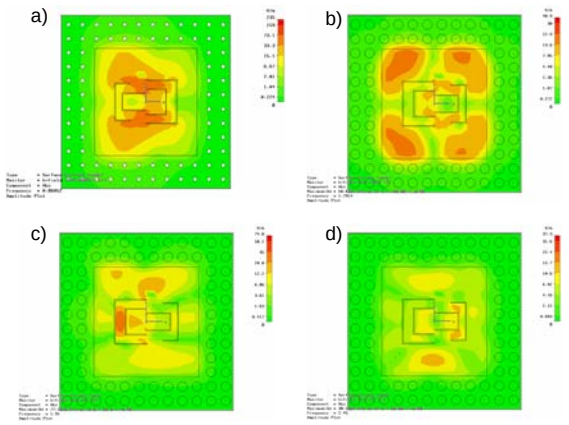

Fig. 15. Current distribution of the prototype 2 on the EBG substrate. The operating frequency: a) 0.86 GHz, b) 1.79 GHz, c) 1.91 GHz, d) 2.45 GHz. Computed by CST Microwave Studio.

Dealing with polarization properties, cross-polarization values in operation frequency bands are given in Tab. 4. Obviously, the prototype 2 on the EBG substrate exhibits the best values.

Frequency	Cross-polarization
0.90 GHz	-21.1 dB
1.80 GHz	-24.8 dB
1.90 GHz	-12.9 dB
2.45 GHz	-12.2 dB

Tab. 4. Cross-polarization for the prototype 2 on the square lattice EBG substrate. Computed by CST Microwave Studio.

Comparisons of the reflection coefficients computed by CST Microwave Studio and measured in an anechoic chamber are given in Fig. 16. Following deviations between results have been obtained: 6.4 % – the first band, 8.0 % – the second one, 3.8 % – the third one, 0.2 % – the fourth one.

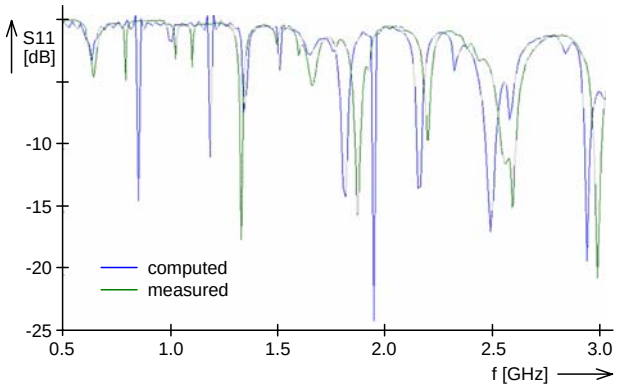

Fig. 16. Frequency response of the reflection coefficient for the prototype 2 on the square lattice EBG substrate (blue – computed by CST Microwave Studio, green – measured).

A positive influence on directivity patterns is not evident in this case: symmetry is slightly worse, and minims in the normal direction stay approximately on the same level.

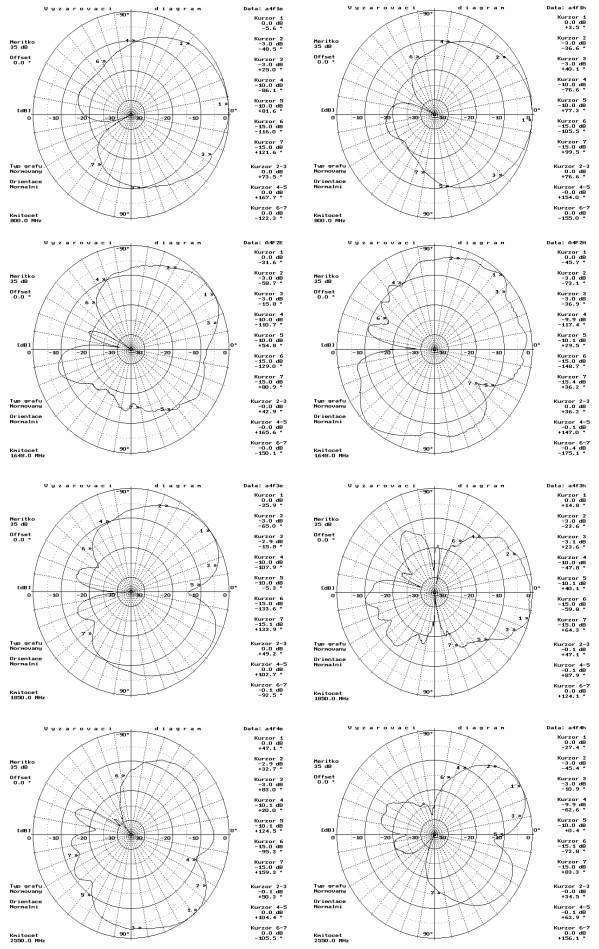

Fig. 17. Measured directivity patterns of the prototype 2 on the EBG substrate in the E-plane (left), and in the H-plane (right), for each frequency band (0.8 GHz, 1.648 GHz, 1.850 GHz, 2.550 GHz), respectively

5. Conclusions

The measured parameters of the investigated antennas are concentrated in Tab. 5. Considering them, following conclusions can be stated:

- EBG antennas provide better gain in all the cases (about 1 dBi maximum).
- The bandwidth of EBG antennas has not been improved. Maybe, the permittivity and height of the substrate have not been satisfactorily high to generate strong enough surface waves.
- Impedance matching of EBG antennas was usually worse compared to conventional ones.
- EBG antennas exhibit lower cross-polarization (Tab. 1 versus Tab. 3, and Tab. 2 versus Tab. 4).

The further development of the described type of antennas is oriented to the association of the parametric antenna model with the multi-objective global optimization routines to improve most antenna parameters by optimizing the antenna layout and the EBG substrate at the same time.

	Prot. 1 conv.	Prot. 1 EBG	Prot. 2 conv.	Prot. 2 EBG
f_1 [GHz]	0.82	0.83	0.80	0.81
B_1 [MHz]	7.00	- - -	1.00	- - -
B_1 [%]	0.85	- - -	0.12	- - -
$s_{11,1}$ [dB]	-7.66	-4.51	-5.35	-2.74
G_1 [dBi]	5.46	6.49	5.76	6.49
f_2 [GHz]	1.80	1.73	1.79	1.65
B_2 [MHz]	47.00	13.00	49.00	- - -
B_2 [%]	2.61	0.75	2.74	- - -
$s_{11,2}$ [dB]	-27.87	-5.43	-10.47	-4.92
G_2 [dBi]	6.57	7.62	6.83	7.56
f_3 [GHz]	1.99	1.93	1.87	1.85
B_3 [MHz]	21.00	67.00	89.00	50.00
B_3 [%]	1.05	3.47	4.75	2.70
$s_{11,3}$ [dB]	-17.60	-24.24	-8.33	-15.27
G_3 [dBi]	7.55	7.63	7.60	8.63
f_4 [GHz]	2.55	2.55	2.46	2.55
B_4 [MHz]	130.00	124.00	107.00	120.00
B_4 [%]	5.09	4.87	4.34	4.70
$s_{11,4}$ [dB]	-19.40	-7.72	-15.30	-14.57
G_4 [dBi]	5.20	6.07	5.25	5.25

Tab. 5. The measured parameters of the investigated antennas: the operation frequency of the m-the frequency band f_m, bandwidth of the m-th frequency band B_m (given by $s_{11} = -5$ dB), reflection coefficient on the m-th operation frequency $s_{11,m}$, and gain on the m-th operation frequency related to the isotropic radiator G_m.

Acknowledgements

Research described in the paper was financially supported by the Czech Grant Agency under the grant no. 102/04/1079, and by the research program MSM 0021630513: Advanced Communication Systems and Technologies.

The study stay of E. Heras and R. Lamadrid at the Brno University of Technology was financed by the Erasmus / Socrates program.

Authors are grateful to Mr. Vítězslav Krčmář (ERA a.s., Pardubice) for measuring antenna prototypes in the anechoic chamber.

References

[1] *CST Reference Manual.* Darmstadt: Computer Simulation Technology, 2005.

[2] *Zeland IE3D Reference Manual*. Fremont: 2005.

[3] *FEMLAB Reference Manual*. Stockholm: COMSOL, 2005.

[4] SAINATI, R. A. *CAD of Microstrip Antennas for Wireless Applications*. Norwood: Artech House, 1996.

[5] GARG, B., BAHL, I. *Microstrip Antenna Design Handbook*. Norwood: Artech House, 2001.

[6] GONZALO, R., NAGORE, G. Simulated and measured performance of a patch antenna on a two dimensional photonic crystals substrate. In *Proceedings of the Progress in Electromagnetics Research Symposium PIERS 2002*. The Electromagnetics Academy, 2002, p. 257–269.

[7] BOUTAYEB, H., DENIDNI, T. A., MAHDJOUBI, K, TAROT, A. C., SEBAK, A. R., TALBI, L. Analysis and design of cylindrical EBG-based directive antenna. *IEEE Transactions on Antennas and Propagation,* 2006, vol. 54, no. 1, p. 211–219.

[8] ABEDIN, M. F., ALI, M. Effects of EBG reflection phase profiles on the input impedance and bandwidth of ultra-thin directional dipoles. *IEEE Transactions on Antennas and Propagation,* 2005, vol. 53, no. 11, p. 3664–3672.

[9] LLOMBART, N., NETO, A., GERINI, G., DE MAAGT, P. Planar circularly symmetric EBG structures for reducing surface waves in printed antennas. *IEEE Transactions on Antennas and Propagation,* 2005, vol. 53, no. 10, p. 3210–3218.

[10] CHEYPE, C., SERIER, C., THEVENOT, M., MONEDIERE, T., REINEX, A., JECKO, B. An electromagnetic bandgap resonator antenna. *IEEE Transactions on Antennas and Propagation,* 2002, vol. 50, no. 9, p. 1285–1290.

[11] FAN, Y., RAHMAT-SAMII, Y. Microstrip antennas integrated with electromagnetic band-gap (EBG) structures: a low mutual coupling design for array applications. *IEEE Transactions on Antennas and Propagation,* 2003, vol. 51, no. 10, p. 2936–2946.

[12] FAN, Y., RAHMAT-SAMII, Y. Reflection phase characterizations of the EBG ground plane for low profile wire antenna applications. *IEEE Transactions on Antennas and Propagation,* 2003, vol. 51, no. 10, p. 2691–2703.

[13] DE MAAGT, P., GONZALO, R., VARDAXOGLOU, Y. C., BARACCO, J. M. Electromagnetic bandgap antennas and components for microwave and (sub) millimeter wave applications. *IEEE Transactions on Antennas and Propagation,* 2003, vol. 51, no. 10, p. 2667 to 2677.

[14] CHAPPELL, W. J., GONG, X. Wide bandgap composite EBG substrates. *IEEE Transactions on Antennas and Propagation,* 2003, vol. 51, no. 10, p. 2744–2750.

[15] LEE, Y. J., YEO, J., MITTRA, R., PARK, W. S. Application of electromagnetic bandgap (EBG) superstrates with controllable defects for a class of patch antennas as spatial angular filters. *IEEE Transactions on Antennas and Propagation,* 2005, vol. 53, no. 1, p. 224–235.

About Authors...

For biographies, see Radioengineering, vol. 14, no. 4, page 20 (December 2005).